Nakahara, Y., Kimura, K., Inokuchi, H., & Yagi, T. (1980) *Chem. Phys. Lett. 73*, 31–34.
Niki, K., Kawasaki, K., Nishimura, N., Higuchi, Y., Yasuoka, N., & Kakudo, M. (1984a) *J. Electroanal. Chem. 168*, 275–286.
Niki, K., Kobayashi, Y., & Matsuda, H. (1984b) *J. Electroanal. Chem. 178*, 333–341.
Niviere, V., Hatchikian, E. C., Bianco, P., & Haladjian, J. (1988) *Biochim. Biophys. Acta 935*, 34–40.
Ono, K., Kimura, K., Yagi, T., & Inokuchi, H. (1975) *J. Chem. Phys. 63*, 1640–1642.
Pierrot, M., Haser, R., Frey, M., Payan, F., & Astier, J. P. (1982) *J. Biol. Chem. 257*, 14341–14348.
Postgate, J. R. (1984) *The Sulphate-reducing Bacteria*, 2nd ed., p 76, Cambridge University Press, Cambridge, U.K.
Ramaprasad, S., Johnson, R. D., & La Mar, G. N. (1984) *J. Am. Chem. Soc. 106*, 3632–3635.
Santos, H., Moura, J. J. G., LeGall, J., & Xavier, A. V. (1984) *Eur. J. Biochem. 141*, 283–296.
Sato, N., Kimura, K., Inokuchi, H., & Yagi, T. (1980) *Chem. Phys. Lett. 73*, 35–35.
Sokol, F., Evans, D. H., Niki, K., & Yagi, T. (1980) *J. Electroanal. Chem. 108*, 107–115.
Tabushi, I., Nishiya, T., Yagi, T., & Inokuchi, H. (1983) *J. Biochem. 94*, 1375–1385.
Verma, A. L., Kimura, K., Nakamura, A., Yagi, T., & Kitagawa, T. (1988) *J. Am. Chem. Soc. 110*, 6617–6623.
Yagi, T. (1984) *Biochim. Biophys. Acta 767*, 288–294.
Yagi, T., & Maruyama, K. (1971) *Biochim. Biophys. Acta 243*, 214–224.
Yagi, T., Honya, M., & Tamiya, T. (1968) *Biochim. Biophys. Acta 153*, 699–705.
Yagi, T., Inokuchi, H., & Kimura, K. (1983) *Acc. Chem. Res. 16*, 2–7.

Identification of Localized Redox States in Plant-Type Two-Iron Ferredoxins Using the Nuclear Overhauser Effect†

L. B. Dugad and Gerd N. La Mar*
Department of Chemistry, University of California, Davis, California 95616
Lucia Banci and Ivano Bertini
Department of Chemistry, University of Florence, 50121 Florence, Italy
Received August 30, 1989; Revised Manuscript Received October 30, 1989

ABSTRACT: The homonuclear Overhauser effect (NOE), in conjunction with nonselective spin–lattice relaxation measurements, has been employed to assign the contact-shifted resonances for the reduced form of two typical plant-type two-iron ferredoxins from the algae *Spirulina platensis* and *Porphyra umbilicalis*. These results demonstrate that the NOE should have broad general applicability for the assignments and electronic structural elucidation of diverse subclasses of paramagnetic iron–sulfur cluster proteins. NOE connectivities were detected only among sets of resonances exhibiting characteristically different deviations from Curie behavior, providing strong support for the applicability of the spin Hamiltonian formulation for the NMR properties of the antiferromagnetically coupled iron clusters [Dunham, W. R., Palmer, G., Sands, R. H., & Bearden, A. J. (1971) *Biochim. Biophys. Acta 253*, 373–384; Banci, L., Bertini, I., & Luchinat, C. (1989) *Struct. Bonding* (in press)]. The geminal β-methylene protons for the two cysteines bound to the iron(II) center were clearly identified, as well as the $C_\alpha H$ and one $C_\beta H$ for each of the cysteines bound to the iron(III). The identification of the iron bound to cysteines 41 and 46 as the iron(II) in the reduced protein was effected on the basis of dipolar contacts between the bound cysteines, as predicted by crystal coordinates of *S. platensis* Fd [Tsukihara, T., Fukuyama, K., Nakamura, M., Katsube, Y., Tanaka, N., Kakudo, M., Wada, K., Hase, T., & Matsubara, H. (1981) *J. Biochem. (Tokyo) 90*, 1763–1773]. Resolved labile proton contact-shifted resonances are attributed to hydrogen bonding to the iron(III) center, and it is concluded that the contact-shifted resonances for the more numerous hydrogen bonds to the iron(II) center are not resolved from the diamagnetic envelope. The identification of the iron closer to the protein surface as the more reducible one is consistent with predictions based on a larger number of hydrogen bonds to this center.

The iron–sulfur proteins comprise a family of proteins with a remarkable variation in both prosthetic group configuration and redox potential (Orme-Johnson & Orme-Johnson, 1982; Thomson, 1985; Jensen, 1987). Except for the unique one-iron rubredoxins, the prosthetic group usually comprises a cluster of two or four irons and an equal number of labile inorganic sulfurs. Although there are now known systems where the terminal amino acid ligands are not cysteine thiolates (Gurbiel et al., 1989), the classical electron-transfer Fe_2S_2, as well as the Fe_4S_4, cluster proteins possess four coordinated cysteines. A number of less regular three-iron clusters have also been characterized recently (Jensen, 1987). One of the remarkable properties of these iron–sulfur cluster proteins is the wide range of redox potential exhibited even within a family of proteins possessing essentially the same cluster (Carter, 1977). Not

† This research was supported by a grant from the National Science Foundation, DMB-87-03611.

0006-2960/90/0429-2263$02.50/0

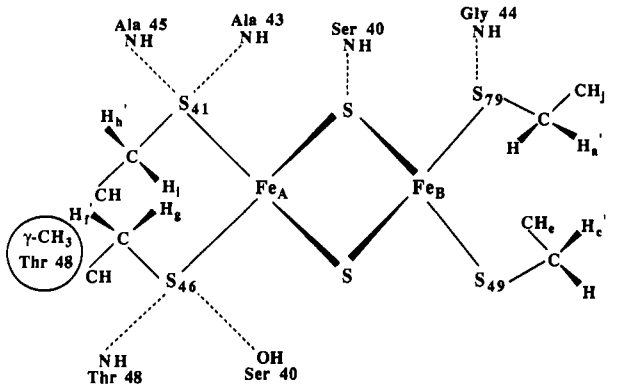

FIGURE 1: Schematic diagram showing the [2Fe-2S] ferredoxin cluster site with two cysteine residues coordinated to each iron atom. The cysteine protons are labeled with a subscript that corresponds to the assigned peaks in the reference spectrum of Figure 2. The potential hydrogen bonds to various sulfur atoms at the cluster site are shown in dotted lines with residue numbers as reported in the crystal structure (Tsukihara et al., 1981).

only are the redox potentials for the clusters modulated by protein interactions, but the potentials of individual components of a cluster can be strongly differentiated to yield localized valence in odd electron states (the two-iron plant and alga ferredoxins) or insignificantly differentiated to produce delocalized valence (the four-iron ferredoxins) (Cammack et al., 1977). The factors that control the redox potential in iron–sulfur proteins are incompletely understood and comprise an area of intense current research. The mechanisms that have been suggested include protein constraints on the cluster geometry (Carter, 1977), aromatic side-chain interaction with the cluster (Markley et al., 1987), hydrogen bonding to the active-site sulfur (Sheridan et al., 1981), and local polarity or dielectric constant (Kassner & Yang, 1977).

One of the simplest systems for studying the control mechanism would be the two-iron, plant-type ferredoxins (Fd)[1] for which the reduced state clearly possesses distinct iron(II) and iron(III) sites that are antiferromagnetically coupled (Dunham et al., 1971; Tsukihara et al., 1987). These are among the strongest reducing agents in biological systems, with a redox potential of ~−400 mV. An X-ray structure of the oxidized algal Fd, *Spirulina platensis*, is available and provides a wealth of structural details on the active site (see Figure 1) (Tsukihara et al., 1981). Theoretical consideration of both hydrogen-bonding interactions (Sheridan et al., 1981) suggested by the crystal structure (Tsukihara et al., 1981) and the local medium dielectricity or polarity (Kassner & Yang, 1977) has led to prediction that the reducing electron is localized on Fe_A (Figure 1). However, an experimental identification of the reduced iron site in these species is still lacking.

^{1}H NMR spectroscopy is ideally suited for characterizing the electronic and molecular structure of iron–sulfur proteins because the hyperfine shift patterns and their temperature dependence provide details of the bonding and the degree of magnetic interactions within the cluster, and a large number of original papers as well as several reviews have appeared in the literature (Phillips & Poe, 1973; Markley et al., 1987; Nagayama et al., 1987). For the two-iron cluster proteins it was recognized early that the hyperfine-shifted proton signals proposed to arise from the coordinated cysteines exhibited two general types of temperature dependence, either weak deviation from Curie dependence ($1/T$), where the shifts decrease with increasing temperature (Curie type), or strong anti-Curie behavior, where the shifts increase with increasing temperature (Dunham et al., 1971; Poe et al., 1971; Salmeen & Palmer, 1972). In an early paper, Dunham et al. (1971) provided a ligand field formulation of the spin coupling between high-spin iron(II) and iron(III) ions that predicted precisely such temperature behavior for the iron(III)- and iron(II)-bound ligands, respectively, and, moreover, predicted that the iron(III) and iron(II) center cysteine contact shifts should differ in magnitude by a factor of ~6. A reformulation and generalization of this treatment has been presented recently that provides similar predictions (Banci et al., 1989). Hence these models suggest that the signals from the two centers should be clearly differentiated by both their shift ranges and their characteristic temperature dependence. For over a decade it was thought that all resolved cysteine peaks resonate in a narrow window 10–45 ppm (Poe et al., 1971; Glickson et al., 1971; Salmeen & Palmer, 1972; Anderson et al., 1975; Chan & Markley, 1983). An important extension of the spectral window was recently reported (Bertini et al., 1984) which showed that there are indeed an additional four nonlabile contact-shifted resonances in the far downfield region, as originally predicted by Dunham et al. (1971), and that both the number of the resonances (four) and their temperature dependence (weak Curie) dictate their origin as the two $C_\beta H_2$ groups of the cysteines bound to the iron(III); what still is not known is to which cysteines the iron(II) or iron(III) is coordinated.

This brings us to the fundamental problem in the interpretation of the ^{1}H NMR spectra of all iron–sulfur proteins, and in particular, for the present two-iron ferredoxins: the assignment of the critical contact-shifted resonances. Elegant model compounds of most of the iron–sulfur proteins have been synthesized (Berg & Holm, 1982), but the ligands dictated by the desired stability outside the protein environment do not possess the same functional group ($-SCH_2$) found in the proteins. To date, assignment strategy for contact-shifted signals has relied largely on intuitive approaches. Definitive assignments require connecting resonances to cysteines with specific neighboring residues identified in the sequence or crystal structure. Such connectivity could be provided by either spin connectivity or dipolar connectivity in the 1-D or 2-D (COSY and NOESY) manifestations (Wüthrich, 1986). While 2-D studies on oxidized protein have made major progress on assignments and structure determination for regions removed from the active site (Markley et al., 1987), the large line widths and rapid relaxation of signals near the iron have precluded detecting the needed connectivities to the bound cysteines.

We have shown recently that the steady-state nuclear Overhauser effect (NOE) (Noggle & Shirmer, 1971) can be effectively utilized to assign resonances in strongly paramagnetic hemoproteins with broad (to 600 Hz) and fast relaxing (T_1 to 2 ms) lines (Unger et al., 1985a; Thanabal et al., 1988). Although the intrinsic (selective) relaxation rate, ρ, is dominated by paramagnetic influences, sufficiently large NOEs are still detectable and can be estimated by conventional relationships:

$$\eta_{i\rightarrow j} = \sigma_{ij}/\rho_j = \sigma_{ij}T_{1j} \quad (1)$$

where $T_1 = \rho^{-1}$ is the selective relaxation time and σ_{ij} is the cross relaxation rate:

$$\sigma_{ij} = -(\hbar^2\gamma_H{}^4/10r_{ij}{}^6)\tau_c \quad (2)$$

with r_{ij} as the interproton distance and τ_c the tumbling time

[1] Abbreviations: NMR, nuclear magnetic resonance; NOE, nuclear Overhauser effect; Fd, ferredoxin; DSS, 2,2-dimethyl-2-silapentane-5-sulfonate; ppm, parts per million; $NADP^+$, nicotinamide adenine dinucleotide phosphate.

of the complex. Since dominance of paramagnetic influences minimizes the difference between the selective and nonselective T_1s (Lecomte & La Mar, 1986), the nonselective T_1 may be used in a strongly paramagnetic complex. For the ~11 000 molecular weight ferredoxins, we estimate $\sigma = -10\ s^{-1}$ using eq 2 for the nearest neighbor (1.77 Å) cysteine β-methylene protons. For nonselective $T_1 \sim 1$–10 ms, eqs 1 and 2 predict $\eta = -1.0$ to −10%, which should be readily detectable even for broad lines, provided the signal to noise (S/N) is sufficient.

We present herein a ^1H NMR NOE study of the two-iron ferredoxins from two highly related algae, *S. platensis* and *Porphyra umbilicalis*, which demonstrates that steady-state NOE assignments allow the identification of hyperfine-shifted CH_2 groups that are bound to the iron(II) and iron(III) centers and that dipolar connectivity between two cysteines coordinated to one of the iron, as well as between a coordinated cysteine and a noncoordinated residue, establishes that the iron(II) in the reduced protein is coordinated by cysteines 41 and 46. The two ferredoxins show a high degree of sequence homology for all residues near the conserved cysteines (Andrew et al., 1976). The strong similarity in their electronic and molecular structures is reflected in their virtually identical NMR spectra (Figure 2). We emphasize here NOE studies on *P. umbilicalis* because of the much more ready availability and better resolution and show that the similarly shifted residues have the same properties in the two proteins, so that the structural interpretation of the NMR spectral features of both ferredoxins can be pursued on the basis of the 2.5-Å resolution X-ray crystal structure of *S. platensis* Fd (Tsukihara et al., 1981).

Materials and Methods

Ferredoxins from *P. umbilicalis* (red alga) and *S. platensis* (blue-green alga) were purchased from Sigma Chemical Co. as salt-free, lyophilized powders and used as received. Tris-$^2H_{11}$ (~99% isotope enriched) was obtained from MSD Isotopes and sodium dithionite ($Na_2S_2O_4$) from J. T. Baker Chemical Co.

The protein samples for NMR experiments were prepared by dissolving 20 mg of ferredoxin in 0.4 mL of ^2H_2O containing 0.5 M Tris-$^2H_{11}$ at pH ~7.5, preadjusted with ^2HCl. The pH values are meter readings not corrected for isotope effects. The protein solution in the NMR tube was bubbled with pure dry nitrogen gas for 2–3 h and then reduced with 0.1 mL of 0.5 M sodium dithionite solution which was previously purged with nitrogen. The reduction was monitored optically on test samples. The final protein concentration was ~4 mM. Reduced ferredoxin samples remained stable for 12-h NMR runs, which required fresh samples each separate day. As many as 20–25 samples were needed to complete all experiments due to repetition and various decoupler controls. The majority of the experiments were carried out on *P. umbilicalis* ferredoxin because of its ready availability in large quantities and slightly better resolved NMR spectrum. To demonstrate the essentially identical results in two different algae, the variable temperature, T_1, and select NOE experiments were carried out on *S. platensis* ferredoxin for which the crystal structure data are available.

Steady-state NOE experiments were performed by using a WEFT pulse sequence (Gupta, 1976) with decoupler irradiation. The selection of τ was such that the residual water signal is nulled at the time of the observe pulse in order to overcome the dynamic range problems while keeping the hyperfine-shifted resonances completely relaxed. Several necessary control experiments were performed by using appropriate decoupler offsets and different irradiation power in order to clearly differentiate between an NOE and an off-resonance saturation effect (Emerson et al., 1988; Thanabal et al., 1986, 1988). The detection of small NOEs in an air-sensitive sample with a large dynamic range poses severe problems. The situation in highly paramagnetic systems is further complicated by having to saturate broad resonances in short times (30–40 ms) and to detect NOEs between closely spaced (in terms of chemical shift) resonances. The use of higher decoupler irradiation power, needed to saturate the resonances, increases the magnitude of off-resonance saturation effects. These problems led to numerous repetitions of each experiment and to alteration of various experimental parameters to confirm the results. To establish the cysteine β-CH_2 proton pairs between peaks f, g, h, and i, several control experiments were required. For example, peak i was saturated and reference spectra were collected with decoupler offsets placed symmetric to peaks f, g, and h; this gave connectivity between peaks h and i. Similar experiments were done to detect reciprocal NOEs, i.e., the NOE from peak h to i (Figure 6). The NOE between peaks f and m (at −0.1 ppm) was monitored over the 15–35 °C range with 5 °C intervals to confirm the NOE to peak m near the diamagnetic region (Figure 5). In all of the NOE experiments, small (−1 to −4%) NOEs could only be detected to the peaks in the 45 to −5 ppm (line widths ~250–300 Hz) region and required 5×10^4 to 3×10^5 scans to achieve the desired signal to noise (S/N). NOEs were not detectable to peaks in the 140–90 ppm region, as the peaks are ≥700 Hz wide and exhibit $T_1 < 2$ ms. The −0.7% inter-cysteine NOE (i.e., between peaks i and g) of iron(II) could only be observed by using a selective (Redfield et al., 1975) excitation pulse sequence in order to optimize the dynamic range.

The ^1H NMR experiments were performed by using a Nicolet NT-360 NMR (360-MHz) spectrometer. The spectra were collected in double precision using 16 384 data points over a 100-kHz bandwidth and placing the carrier frequency at the residual solvent resonance. The resonance of interest was irradiated for time $t \gg T_1$ (usually 30–40 ms), which guarantees the steady-state condition, with a 100-ms repetition time. The spectra were collected in interleaved fashion with decoupler irradiation applied on- and off-resonance. The NOE difference spectrum was obtained by subtracting the off-resonance spectrum from on-resonance saturation. The free induction decays were apodized to improve the S/N, resulting in 50–100-Hz line broadening. The chemical shifts are referenced to the residual water signal, which in turn was calibrated against internal 2,2-dimethyl-2-silapentane-5-sulfonate (DSS). Chemical shifts are reported in parts per million (ppm) with downfield shifts taken as positive. The spectra in ^1H_2O solution were collected by Redfield selective excitation by placing the carrier frequency at the region of interest. The relaxation experiments in ^1H_2O solution were performed by using the WEFT pulse sequence (Gupta, 1976) and collecting spectra at various τ values. The nonselective T_1s were determined by using the inversion–recovery sequence, and data were analyzed by using a three-parameter nonlinear least-squares fit with programs available on Nicolet software.

Results

The ^1H NMR spectra of the reduced Fd from *S. platensis* and *P. umbilicalis* in ^2H_2O at 30 °C are illustrated in parts A and C, respectively, of Figure 2; the traces of the same two reduced Fd complexes in ^1H_2O are shown in parts B and D, respectively. In addition to the previously reported resonances in the window 45 to −5 ppm in ^2H_2O (Poe et al., 1971; Glickson et al., 1971; Slameen & Palmer, 1972; Anderson et

Table I: ^1H NMR Spectral Parameters for Resolved Resonances of Reduced Two-Iron Ferredoxins[a]

peak	assignment[b]		*P. umbilicalis* Fd		*S. platensis* Fd	
			shift (ppm)	T_1 (ms)	shift (ppm)	T_1 (ms)
a	Cys 79(?)	$C_\beta H'$[c]	130.9	1.2 ± 0.2	134.4	1.3 ± 0.2
b	Cys 49 or 79	$C_\beta H$	122.6	0.3 ± 0.1	124.9	0.4 ± 0.1
c	Cys 49(?)	$C_\beta H'$	103.8	1.4 ± 0.2	103.2	1.5 ± 0.2
d	Cys 79 or 49	$C_\beta H$	97.5	0.4 ± 0.1	97.4	0.5 ± 0.1
e	Cys 49(?)	$C_\alpha H$	43.12	5.4 ± 0.5	43.20	5.2 ± 0.5
f	Cys 46	$C_\beta H'$	27.56	8.0 ± 0.8	26.40	7.7 ± 0.7
g	Cys 46	$C_\beta H$	26.65	5.6 ± 0.5	25.80	5.5 ± 0.5
h	Cys 41	$C_\beta H'$	22.04	10.8 ± 1.0	21.13	11.0 ± 1.0
i	Cys 41	$C_\beta H$	18.60	3.6 ± 0.3	17.90	4.0 ± 0.4
j	Cys 79(?)	$C_\alpha H$	17.60	5.6 ± 0.5	17.90	5.6 ± 0.5
k			12.24	7.7 ± 0.8	12.32	7.8 ± 0.8
l	Pro 38(?)		2.2	*d*		
m	Thr 48(?)	CH_3	−0.15	~70	−0.10	~70
n and p	Arg 42(?)		−2.48	3 ± 0.3	−2.60	3 ± 0.3
q	Gly 44 or Ser 40(?)	N_pH	(−15.3)[e]	~2	−15.0	~2
r	Gly 44 or Ser 40(?)	N_pH			−16.4	~2

[a] At 30 °C; pH 7.0 in ^2H_2O (except in ^1H_2O for exchangeable proton resonances, q and r). [b] Assignment designated (?) are only tentative. [c] $C_\beta H$ is always closer to the bound iron than $C_\beta H'$. [d] Not resolved. [e] The two labile proton peaks overlap.

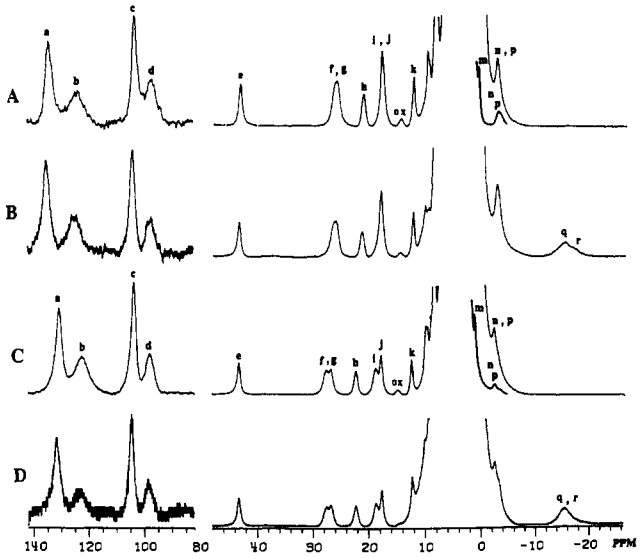

FIGURE 2: Hyperfine-shifted region of the 360-MHz ^1H NMR spectrum of reduced ferredoxin at 30 °C, pH = 7.5, from *S. platensis* (A) in ^2H_2O and (B) in 90% H_2O/10% ^2H_2O; and from *P. umbilicalis* (C) in ^2H_2O and (D) in 90% H_2O/10% ^2H_2O; exchangeable protons q and r are seen in (B) and (D). The upfield section, 0 to −5 ppm, is also shown at $^1/_8$ vertical expansion to identify the three-proton methyl signal m. The 80–140 ppm region is expanded 5 times vertically to clearly show the broad peaks a–d.

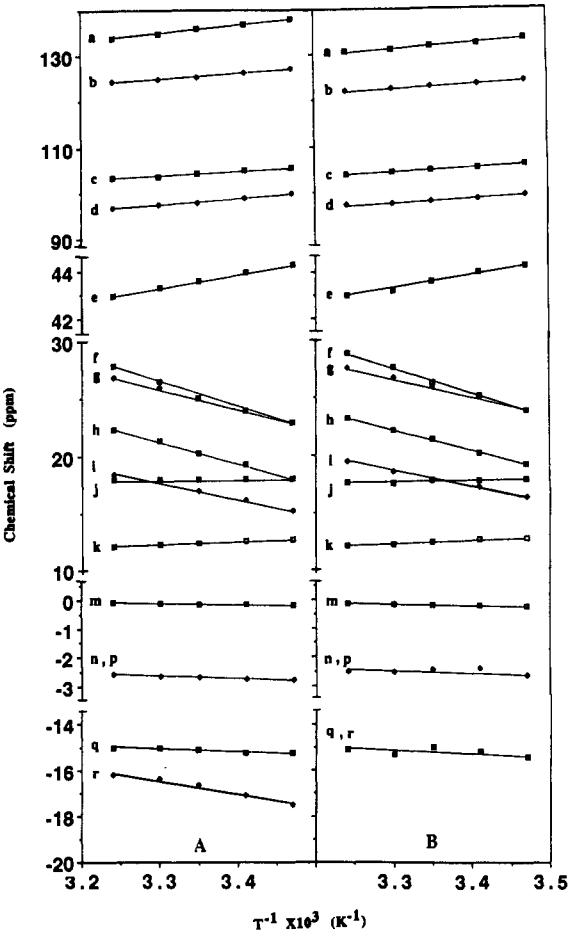

FIGURE 3: Curie plots for hyperfine-shifted resonances of reduced ferredoxin from (A) *S. platensis* and (B) *P. umbilicalis* ferredoxin, with peaks labeled as in Figure 2. The solid lines only indicate the trends and are not fits to the experimental data.

al., 1975; Chan & Markley, 1983), we find the expected four broad single proton peaks a–d in the region 110–140 ppm that must originate from the iron(III) $C_\beta H_2 S$ (Dunham et al., 1971; Bertini et al., 1984; Banci et al., 1989), as well as previously unreported upfield-shifted exchangeable proton signals, q and r, near −15 ppm. All chemical shift data are listed in Table I. In *S. platensis* in ^1H_2O, two distinct labile proton peaks, q and r, with apparent single-proton intensity are partially resolved with different line widths (Figure 2B); for *P. umbilicalis*, a single broad resonance is observed with area for two protons (Figure 2D). A nonexchangeable signal on the upfield side of the diamagnetic envelope, peak m, exhibits three-proton intensity when compared to that of a single-proton low-field resonance e–j, as concluded for a spectral simulation using the standard Nicolet program. This three-proton peak, moreover, revealed a single, symmetricl Lorentzian peak over the temperature range 5–35 °C, indicating that it originates from a single methyl group. The resonance at ~−2.5 ppm has two-proton intensity, n and p, and is only partially resolved for *P. umbilicalis* Fd, as shown in Figure 2C,D. The temperature dependences for all resolved resonances of both reduced Fds are illustrated in Figure 3 in the form of a Curie plot (shift versus reciprocal temperature).

The relaxation times obtained from the nonselective inversion–recovery experiments for the two reduced proteins are included in Table I. T_1 values for the single-proton resonances

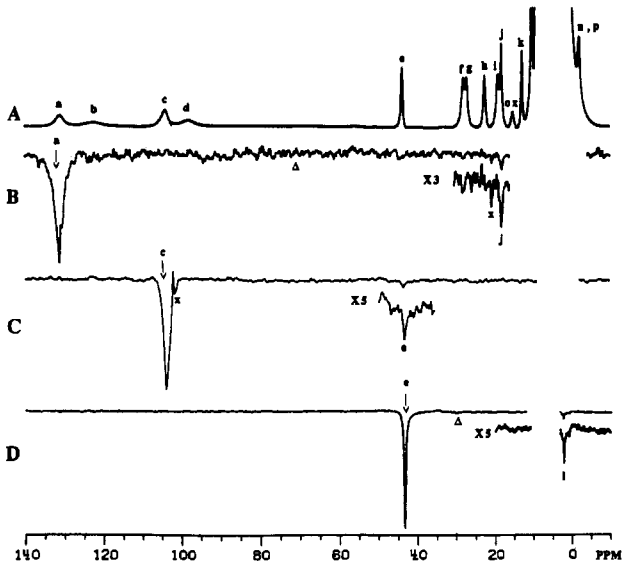

FIGURE 4: (A) ^1H NMR spectrum of reduced ferredoxin from *P. umbilicalis* in ^2H_2O, pH = 7.5, 30 °C. (B–D) Difference traces for on-resonance saturation (position marked by ↓) minus off-resonance (position marked by Δ if in shown spectral window) of peaks. (B) Saturated peak a with decoupler at 70 ppm in reference trace; note ~−1.5% NOE to peak j. (C) Saturated peak c with decoupler at 170 ppm in reference trace; note ~−2% NOE to peak e. (D) Saturated peak e with decoupler at 30 ppm in reference trace; note NOE to peak l at 2.2 ppm. Experimental artifacts (glitches) are labeled x; the diamagnetic region, 3–6 ppm, is obliterated by incomplete cancellation of the residual solvent and intense diamagnetic envelope.

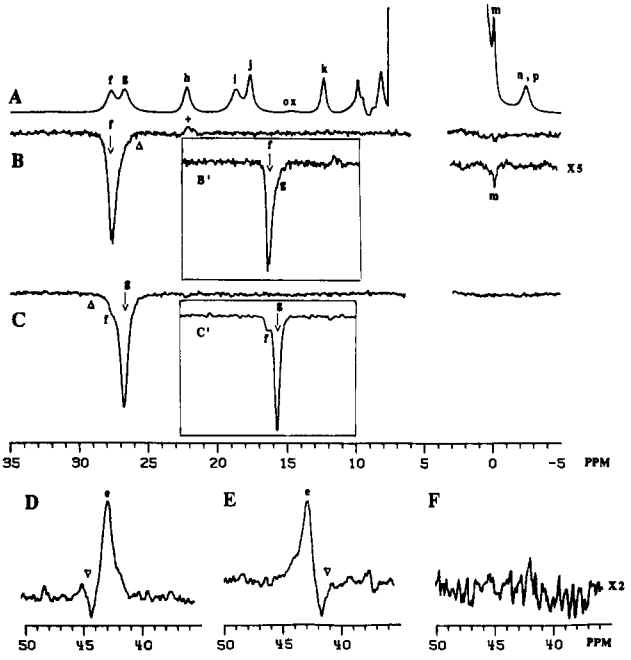

FIGURE 5: (A) 35 to −5 ppm region of the ^1H NMR spectrum of reduced ferredoxin from *P. umbilicalis* in ^2H_2O, pH = 7.5, 30 °C. (B) Difference trace upon partial (~50%) saturation of peak f with decoupler in reference trace symmetric to peak g; note that peak f in the difference trace is unsymmetrical, with area at position of peak g. Simulation of the asymmetry indicates a ~−7% NOE to peak g. Note also small NOE from f to peak m. (C) Difference trace upon partial saturation (~50%) of peak g; note intensity for peak f. Simulation indicates a ~−10% NOE to peak f. The insets B′ and C′ show double-exponential resolution-enhanced region of difference traces B and C, respectively. That the off-resonance saturation of peaks g and f in traces B and C, respectively, does not contribute to the intensity for those peaks in the difference traces is illustrated in traces D and E, where we show the traces resulting from the decoupler placed 1 ppm to the low-field (D) and high-field (E) side of peak e (decoupler position marked Δ), both of which exhibit clear off-resonance saturation of peak e, but which completely cancels in the *difference* between traces D and E, as shown in trace F (vertical expansion × 2 that in D and E). Hence, off-resonance effects between peaks f and g are negligible in traces B and C.

range from 3 to 11 ms in the 10–45 ppm range and suggest that steady-state NOEs between geminal protons resonating in this window should be readily detectable. The low-field iron(III) $C_\beta H_2$ signals relax faster, with only crude T_1 estimates available for the two broadest peaks, b and d. The exchangeable peaks in ^1H_2O were estimated to have $T_1 \sim 1$–2 ms; their line widths (~600 Hz) are also similar to the low-field peaks a and c.

The observed dipolar connectivities are presented for reduced *P. umbilicalis* Fd, but essentially the same connectivities were observed between similarly labeled peaks for *S. platensis* Fd. Saturation of the broad peaks, a and c (700–800 Hz at 360 MHz), failed to yield detectable NOEs between them or to peaks b and d (1.4–1.5 kHz). However, the very short T_1s for peaks b and d would preclude detection of the predicted ~−0.4% NOE via eqs 1 and 2 for the closest β-methylene proton pair at the attainable S/N. Hence the presence or absence among peaks a–d of the dipolar connectivity for a methylene group could not be established. We note, however, that saturation of peak a (Figure 4B) yields a small, ~−1.8% NOE to peak j, which with the T_1 = 5.6 ms for peak j translates into a distance $r_{aj} \sim 2.1$ Å. Similarly, irradiation of peak c yields a ~−1.5% NOE to peak e (Figure 4C); the $T_1 \sim 5.4$ ms results in $r_{ce} \sim 2.2$ Å. Partial saturation (≲20%) of peak b or d failed to yield detectable (>|1%|) NOEs to any resolved resonance. Irradiation of peak j failed to yield a detectable NOE (not shown), while the saturation of peak e (Figure 4D) yields a small NOE in the unresolved diamagnetic envelope to peak l at 2.2 ppm.

Saturation of peak f yields a difference trace (Figure 5B) with ~−7% intensity for peak g, as revealed by spectral simulation of the asymmetric resonance. Carrying out the reverse experiment by saturating peak g yields considerable intensity (~−10%) for peak f in the difference trace (Figure 5C), consistent with their relative T_1 values. In each case the decoupler in the reference trace was placed symmetrical to the peak being detected so as to cancel any off-resonance saturation effects on the detected peak. That such off-resonance effects cancel if there is no dipolar connectivity is demonstrated by the experimental results described in parts D–F of Figure 5, where placing the decoupler 1.0 ppm to the left (Figure 5D) and right (Figure 5E) of peak e yields substantial off-resonance effects on peak e that completely vanish in their difference trace (Figure 5F). The available signal to noise is such that a 2% off-resonance effect could readily be detected. The intensities for the detected peaks in traces B and C of Figure 5 are much larger than this (~7 and 10%, respectively), such that off-resonance effects make only minor contributions. Hence the intensity of peaks g and f in traces B and C, respectively, of Figure 5 must arise from true NOEs. The ~−10% $\eta_{g\to f}$ translates to $r_{gf} \sim 1.8$ Å with the T_1 at 8.0 ms for peak f; hence peaks f and g must be geminal methylene protons. It is also observed in Figure 5B that saturation of peak f (but not peak g in Figure 5C) yields a small NOE to peak m; this NOE tracks the three-proton peak, m, in the temperature range 5–35 °C and hence reflects an NOE to a methyl peak with $T_1 \sim 70$ ms. Irradiation of peak i leads to a ~−14% NOE for peak h, as shown in Figure 6B; the decoupler in the reference trace is symmetrical to peak h (position marked Δ) and causes partial saturation of peaks g and f (positive intensity). The reciprocal ~−5% NOE for peak h to i is shown in Figure 6C. Each of these NOEs yields $r_{hi} \sim$

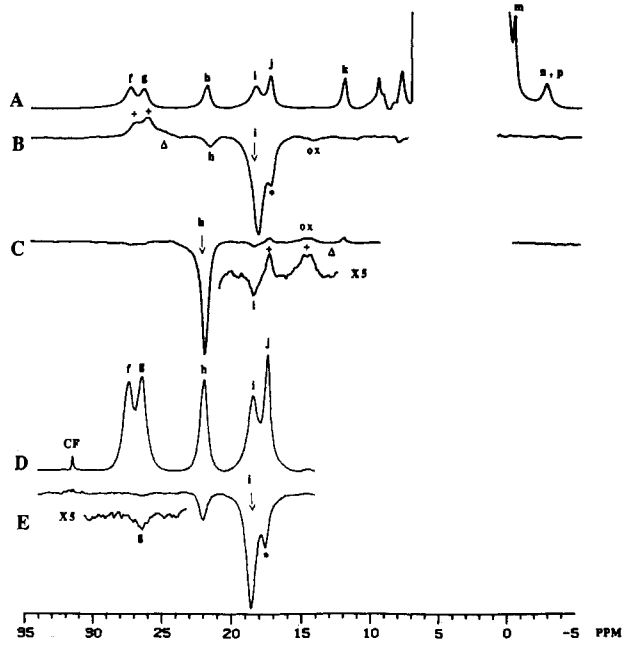

FIGURE 6: (A) 35 to −5 ppm region of the normal ^1H NMR spectrum of reduced ferredoxin from *P. umbilicalis* in ^2H_2O, pH = 7.5, 30 °C. (B) Difference spectrum upon partial saturation of peak i with decoupler in reference trace symmetric to peak h (marked by Δ); note ~−14% NOE to peak h. (C) Difference trace upon partial (~80%) saturation of peak h with decoupler in reference trace symmetrical to peak i (marked Δ); note ~−5% NOE to peak i. (D) The spectral region between 35 and 15 ppm obtained with selective Redfield detection by placing carrier frequency at 32 ppm (position indicated by CF). (E) The difference Redfield trace upon partially (~50%) saturating peak i with decoupler placed symmetric to peak g at 37 ppm to eliminate off-resonance effects to peak g; note ~−0.7% NOE to peak g. Off-resonance-saturated peaks in the master trace (same phase as directly saturated peaks) and in the reference trace (phase inverted from that of directly saturated peak) are marked * and +, respectively.

1.8 Å when the measured T_1s in Table I are used. Hence peaks h and i comprise yet another set of geminal methylene protons. No NOEs could be detected to peaks in the diamagnetic envelope, 0–10 ppm, when either peak h or peak i was saturated, although artifacts obscure the 3–6 ppm portion. Finally, Figure 6E shows ~−0.7% NOE between inter-cysteine $C_\beta H$ proton peaks i and g with $r_{ig} \sim 2.7$ Å. Saturation of the upfield exchangeable resonances of *P. umbilicalis* Fd in ^1H_2O failed to yield any detectable NOEs (not shown).

Discussion

Assignment of Resonances to the Discrete Oxidation States. The theoretical models (Dunham et al., 1971; Banci et al., 1989) argue the contact shifts for all resonances exhibiting weak Curie behavior (peaks a–d, e, j, k, m, n, and p) as arising from the spin magnetization of the iron(III) center, and those displaying strong anti-Curie behavior (f–i) as originating from the iron(II) center. The four far downfield single proton peaks a–d must certainly originate from the two $C_\beta H_2$s of the iron(III) center. The X-ray structure yields iron–proton distances (≲4.0 Å) to the nonequivalent Fe_A and Fe_B (Figure 1) as listed in Table II (Tsukihara et al., 1981); thus each cysteine has one $C_\beta H$ much closer to the bonded iron than its geminal partner, $C_\beta H'$, leading to the expectation, at least for iron(III) bound cysteines, that $C_\beta H$ is the faster relaxing of a geminal methylene pair. Moreover, in each case, the crystal coordinates indicate very similar and much shorter distances between $C_\beta H'$ and $C_\alpha H$ (~2.5 Å) than between $C_\beta H$ and $C_\alpha H$ (~3.0 Å) on the same residue. Hence $C_\beta H' \rightarrow C_\alpha H$ NOEs

Table II: Cysteine Proton–Iron Distances from the Crystal Structure of *S. platensis* Ferredoxin[a]

	Cys 41			Cys 46		
	$C_\beta H$	$C_\beta H'$	$C_\alpha H$	$C_\beta H$	$C_\beta H'$	$C_\alpha H$
Fe_A[b]	3.0	4.0	4.3	2.8	4.0	4.8
Fe_B	5.5	6.1	6.3	4.9	5.7	5.6
	Cys 49			Cys 79		
	$C_\beta H$	$C_\beta H'$	$C_\alpha H$	$C_\beta H$	$C_\beta H'$	$C_\alpha H$
Fe_A	3.8	4.1	6.5	5.1	5.8	7.7
Fe_B	2.4	2.9	4.8	3.2	4.0	5.5

[a] In Å, from the X-ray crystal coordinates as determined by Tsukihara et al. (1981). [b] Iron center is defined in Figure 1; Fe_A = iron(II) and Fe_B = iron(III) in reduced Fd.

should be much larger than $C_\beta H \rightarrow C_\alpha H$ NOEs. The NOE between peaks a → j and c → e and resulting distances (2.2–2.3 Å) indicate that peaks a, j and c, e arise pairwise from $C_\beta H'$, $C_\alpha H$ of the two cysteines attached to iron(III), with peaks b and d comprising the remaining $C_\beta H$s.

The pair of peaks f, g and h, i have NOEs between them that indicate a pair of geminal proton sets ($r_{fg} \sim r_{hi} \sim 1.8$ Å) and hence must arise from the $C_\beta H_2$s of the two cysteines bound to iron(II). Thus strong dipolar connectivity is observed solely among sets of resonances with either weak Curie or strong anti-Curie behavior and provides the first experimental confirmation for the predictions (Dunham et al., 1971; Banci et al., 1989) that the characteristic deviations from Curie behavior of contact-shifted resonances can be used to differentiate between resonances from the two distinct localized valence states of the two-iron ferredoxins. Saturation of peaks f–i failed to yield detectable NOEs to the remaining unassigned resolved proton resonances, k, n, and p, establishing that none of the latter arise from the $C_\alpha H$ of iron(II)-bound cysteines. The failure to detect any clear NOEs in the diamagnetic envelope suggests that the two $C_\alpha H$s likely resonate near the residual solvent signal whose off-resonance saturation tends to obscure the difference traces in the 3–6 ppm region.

Identification of Individual Iron Sites. This involves the unambiguous assignment of at least one of the eight cysteine $C_\beta H$s by NOE, either a unique contact to an assignable proton signal from a neighboring noncoordinated residue or a unique inter-cysteine contact. The X-ray crystal structure of *S. platensis* Fd (Tsukihara et al., 1981) reveals that proton–proton distances between two bound cysteines are always >3.7 Å and, hence, too far to yield detectable NOEs, with the sole exception of the $C_\beta H$s closest to the iron of the two cysteines 41 and 46, for which the distance is only 2.7 Å, so that a ~−0.3 to −0.8% interresidue NOE can be expected, depending on the T_1 value. On this premise, we searched carefully for NOEs between the two geminal methylene proton sets f, g and h, i. No such NOE could be detected between either h or i and f (not shown); however, saturation of peak i yields a definite small ~−0.7% NOE (see Figure 6E) which translates to $r_{ig} \sim 2.7$ Å when T_1(g) = 5.2 ms is used. This unambiguously establishes that peaks h, i and f, g arise from cysteine $C_\beta H_2$s attached to one center and that this center has one $C_\beta H$ within 2.7 Å of the second coordinated cysteine β-CH. *We therefore identify the iron(II) localized valence with the iron attached to cysteines 41 and 46, leaving cysteines 49 and 79 coordinated to the iron(III) center.*

The detection of an NOE from peak f (but not g) to the slightly upfield-shifted methyl peak m (Figure 5B) suggests a basis for differentiating between the Cys 41 and Cys 46 signals. The closest methyls in the crystal structure to Cys 41 $C_\beta H$ are 5.2 Å (Ala 43), while Cys 46 has Thr 48 $C_\gamma H_3$

only 3.1 Å from $C_\beta H'$ and 4.0 Å from $C_\beta H$. This leads to the assignments that signals f, g and h, i originate from Cys 46 and Cys 41, respectively, bound to the iron(II) center. The individual cysteine signals coordinated to iron(III) are more difficult to identify. The only detected NOE from peak e to peak l at 2.2 ppm cannot be assigned, although it could arise from a Pro 38 proton close to Cys 49. We note that, although the NOE pattern solely among the peaks f–i, together with the crystal coordinates, establishes them as originating from C_βHs on Cys 41 and Cys 46, the assignment of the oxidation state still rests on the ligand field theory for the contact shifts for the spin-coupled centers (Dunham et al., 1971; Banci et al., 1989). Both contact and dipolar shifts are proportional to $\langle S_z \rangle$. The theoretical treatments predict $\langle S_z \rangle_{Fe(III)}/\langle S_z \rangle_{Fe(II)} \sim 6$ (Dunham et al., 1971; Banci et al., 1989). The present contact shifts for assigned C_βHs of iron(III) (peaks a–d, mean contact shift ~110 ppm) and iron(II) (peaks f–i, mean contact shifts ~20 ppm) yield a $\langle S_z \rangle$ ratio of ~5.5. The remarkable consistency between the predictions on relative shift magnitudes and temperature dependence for the two localized valence states and the experimental data for the presently assigned resonances provides strong confirmation for this theoretical model. The present NOE data demonstrate clearly that definitive resonance assignments for the hyperfine-shifted resonances in a variety of iron–sulfur proteins should now be possible. The geminal methylene proton pairs for the bound cysteines in weakly paramagnetic four-iron ferredoxins have thus been identified (I. Bertini, F. Briganti, C. Luchinat, and D. Scozzafava, submitted for publication).

The much larger $\langle S_z \rangle$ for the iron(III) than iron(II) center indicates that the dipolar shifts (Jesson, 1973; Bertini & Luchinat, 1986) for any noncoordinated residue are likely to reflect a temperature dependence dominated by the iron(III) center even though it may, in fact, be closer to the iron(II) than the iron(III) center. Peaks k, m, n, and p all exhibit weak Curie-type behavior (Figure 3). Since peaks a–e and j account for all six nonlabile protons of the two cysteines bound to iron(III), the weakly shifted peaks, k, m, n, and p must arise from some noncoordinated amino acid side chain that senses primarily dipolar shifts from the iron(III). The nonassigned but relatively efficiently relaxed signals, n and p, possibly arise from protons close to the iron centers, such as the Arg 42 which has protons only 3.2 Å from both Fe_A and Fe_B. The proximity of the diamagnetic envelope precluded effective saturation of signals k, n, and p without causing unacceptable off-resonance excitation of the diamagnetic envelope, and hence these signals remain unassigned.

Relaxation of Contact-Shifted Resonances. Nuclear relaxation is strongly affected by interaction with unpaired electron(s). Tetrahedral, high-spin iron(III) generally exhibits slow electron spin relaxation ($\tau_s \sim 10^{-11}$ s) which produces very broad ^{1}H NMR lines. Indeed, the coordinated cysteine protons are not detected in the Fe(III)S_4 rubredoxin; high-spin iron(II), on the other hand, possesses a shorter relaxation time ($\tau_s \sim 10^{-12}$–10^{-13} s) and hence yields lines sufficiently narrow to detect in the reduced rubredoxin (Werth et al., 1987). Magnetic coupling between a set of fast and slowly relaxing spins causes a large increase in the relaxation rate for the slower relaxing center as long as the magnetic coupling, J, is larger than $\hbar\tau_s$ for the slow relaxing metal ion (Banci et al., 1988), as is known to be the case for the present Fd (Palmer et al., 1971). Nuclear relaxation due to coupling with the unpaired electron is proportional to $\langle S^2 \rangle$ and a spectral density function, $f(\tau_s,\omega)$, where ω = the Larmor frequency. In a magnetically coupled system, Fe_A·Fe_B, $\langle S'^2 \rangle_A$ and $\langle S'^2 \rangle_B$ are evaluated over the accessible new levels, S_i', of the pair (Banci et al., 1989). The relative importance of relaxation effects is further influenced by the distance of a given proton from the two iron centers, and the relaxation rate is the sum of the contributions from the two centers. The calculated ratio between $\langle S'^2 \rangle_{Fe(III)}$ and $\langle S'^2 \rangle_{Fe(II)}$ for the present system (J = 100 cm^{-1}, 303 K) is 4.6. The experimental values, even if they are allowed for the different distances of the protons from the metal ions, indicate that the ratio of T_1s for Fe(III) and Fe(II) Cys protons similarly disposed to their bound iron is somewhat larger (5–19) than 4.6, but is within a factor of 2 for three of the four Cys C_βHs. This is possibly due to the fact that the electronic correlation time for Fe^{3+} is slightly longer than that for Fe^{2+}.

The presence of one broad and fast relaxing peak (b or d) and one narrow and more slowly relaxing peak (a or c) for the C_βHs of the iron(III)-bound Cys 49 or 79 is qualitatively consistent with the configuration of the ligands that places one $C_\beta H$ ~0.5 Å closer to the iron for each of the four cysteines. However, the C_αHs (peaks e and j) of both Cys 49 and Cys 79 appear too strongly relaxed compared to their prediction based on R_i^{-6}, suggesting possibly important influence from relaxation by delocalized spin density (Unger et al., 1985b; Banci et al., 1987). The strong possibility of large contributions from ligand-centered effects on T_1 is also suggested by the relaxation data for the four iron(II)-bound cysteine C_βHs. Thus the distances to the iron for $C_\beta H$ and $C_\beta H'$ for Cys 41 and Cys 46 predict T_1 ratios ~7–10 (Table II). In practice, this ratio could be higher because the $C_\beta H$ close to bonded Fe(II) is also closer to the Fe(III). We observe a ratio of only 1.4–3.0 (Table I). The apparent absence of iron(III) relaxation influences on peaks f–i suggests that the relation by the iron(III) center may be much less than reflected by the iron(III)-bound cysteine $C_\beta H$ T_1s. Hence analysis of differential relaxation rates via the conventional relation, $T_{1i}/T_{1j} = R_i^6/R_j^6$ (Bertini & Luchinat, 1986), using the T_1 for a Cys H_β will lead to large overestimation of iron–proton distances for noncoordinated residues.

Hydrogen Bonding to the Cluster. We observe two exchangeable proton resonances resolved from the diamagnetic envelope. Their line widths (~600 Hz) and estimated T_1s (1–2 ms) are similar to those of peaks a and c, and this suggests that they are likely comparably close to the iron(III) center (~4 Å). Since the peptide NH of the coordinated Cys are ≥5 Å from either iron center, these signals must represent contact shifts for labile protons involved in hydrogen bonds to bound sulfur. Similarly, upfield-shifted labile proton peaks have been previously identified for the high-potential iron proteins, HiPIPs (Krishnamoorthi et al., 1986). The crystal structure of *S. platensis* Fd (Tsukihara et al., 1981) has been interpreted as reflecting six hydrogen bonds to the cluster, four to the bound Cys of Fe_A, one to Cys 79 of Fe_B (NH of Gly 44), and one primarily to the bridging sulfur (NH of Ser 40). The variable-temperature plots for labile protons peaks q and r (Figure 3) exhibit the weak Curie behavior (shifts increase as temperature decreases), confirming that protons q and r experience comparable amounts of spin density reflecting overwhelmingly the iron(III) center $\langle S_z \rangle$. This leads to the tentative assignment of peaks q and r to the peptide NHs of Ser 40 and Gly 44. The distances from the iron(III) center for these H-bonding protons are not obtainable directly from the X-ray coordinates; however, the existence of hydrogen-bonding interactions with the S should bring them within ~4 Å from the iron(III).

The question naturally arises as to where one would expect to detect the four contact-shifted resonances for the labile protons that participate in the four hydrogen bonds to cysteines 41 and 46 bound to iron(II). Using the relative Cys $C_\beta H$ contact shift as a guide that indicates $\langle S_z \rangle$ is ~5.5 larger for iron(III) than iron(II), the upfield shifts for the labile protons for iron(II) are likely to be only ~5 ppm, which would not allow their resolution from the diamagnetic envelope.

The present NMR study demonstrates that the residues projected to serve as hydrogen bond donors to the bound sulfur do in fact participate in such an interaction (Tsukihara et al., 1981). Previously such contact shifts arising from hydrogen bonding had been observed only for four-iron systems (Krishnamoorthi et al., 1986). Moreover, this iron site (Fe_A) identified with the reducing electron is the one that is involved in four hydrogen bonds, as opposed to only one to the ferric (Fe_B) center. In the absence of any π interaction with aromatic side chains, this supports the proposals (Carter, 1977) that hydrogen bonding is the major determinant of redox potential in the two-iron proteins. The presence of such hydrogen bonding has been indirectly inferred previously on the basis of the observation of isotope effects on the resonance Raman lines of *S. platensis* Fd (Sanders-Loehr, 1988). The location of the reducing electron on the iron closer to the protein surface is also consistent with dielectric medium stabilization and likely contributes to facile electron transfer to the ferredoxin–$NADP^+$ reductase (Tsukihara et al., 1987). For the four-iron HiPIP system, it has been argued that, while hydrogen bonding is an important fact, the π interaction with adjacent aromatic rings also modulates the relative stabilities of the ferric and ferrous states (Krishnamoorthi et al., 1986).

Conclusions

The present NMR experiments demonstrate that steady-state NOE can be observed in the reduced two-iron ferredoxins with T_1s in the range 2–10 ms and that the magnitude of the NOEs allows identification of the protons for individual cysteines. Thus similar NOE studies should have considerable power for eventually providing the critically needed assignments that will help unravel the NMR spectra of more complicated iron–sulfur proteins. Preliminary results in our laboratory indicate that the present NOE studies have direct applicability even to the substantially larger and more complex nitrogenase iron–sulfur protein cofactor (J. B. Howard, L. B. Dugad, and G. N. La Mar, unpublished data). For the plant-type ferredoxins, we identify the ferrous site with the iron A, bound by cysteines 41 and 46; this is consistent with the lower redox potential for site A being determined by the larger number of hydrogen-bonding interactions to its coordinated sulfurs, as predicted earlier (Carter, 1977).

Acknowledgments

We are indebted to V. Thanabal, W. O. Parker, Jr., J. S. de Ropp, and S. W. Unger for assistance with the preliminary NOE experiments, to A. L. Balch for making available preparative apparatus, and to C. Luchinat for useful discussions.

References

Anderson, R. E., Dunham, W. R., Sands, R. H., Bearden, A. J., & Crespi, H. L. (1975) *Biochim. Biophys. Acta 408*, 306–318.

Andrew, P. W., Rogers, L. J., Boulter, D., & Haslett, B. G. (1976) *Eur. J. Biochem. 69*, 243–248.

Banci, L., Bertini, I., Luchinat, C., & Scozzafava, A. (1987) *J. Am. Chem. Soc. 109*, 2328–2334.

Banci, L., Bertini, I., & Luchinat, C. (1988) in *Metal Clusters in Proteins* (Que, L., Jr., Ed.) Chapter 4, American Chemical Society, Washington, DC.

Banci, L., Bertini, I., & Luchinat, C. (1989) *Struct. Bonding* (in press).

Berg, J. M., & Holm, R. H. (1982) in *Iron–Sulfur Proteins* (Spiro, T. G., Ed.) pp 1–67, Wiley-Interscience, New York.

Bertini, I., & Luchinat, C. (1986) *NMR of Paramagnetic Molecules in Biological Systems*, Benjamin/Cummings, Menlo Park, CA.

Bertini, I., Lanini, G., & Luchinat, C. (1984) *Inorg. Chem. 23*, 2729–2730.

Cammack, R., Dickson, D. P. E., & Johnson, C. E. (1977) in *Iron–Sulfur Proteins* (Lovenberg, W., Ed.) Vol. III, pp 283–330, Academic, New York.

Carter, C. W., Jr. (1977) *J. Biol. Chem. 252*, 7802–7811.

Chan, T.-M., & Markley, J. L. (1983) *Biochemistry 22*, 6008–6010.

Dunham, W. R., Palmer, G., Sands, R. H., & Bearden, A. J. (1971) *Biochim. Biophys. Acta 253*, 373–384.

Emerson, S. D., Lecomte, J. T. J., & La Mar, G. N. (1988) *J. Am. Chem. Soc. 110*, 4176–4182.

Glickson, J. D., Phillips, W. D., McDonald, C. C., & Poe, M. (1971) *Biochem. Biophys. Res. Commun. 42*, 271–279.

Gupta, R. K. (1976) *J. Magn. Reson. 24*, 461–465.

Gurbiel, R. J., Batie, C. J., Sivaraja, M., True, A. E., Fee, J. A., Hoffman, B. M., & Ballou, D. P. (1989) *Biochemistry 28*, 4861–4871.

Jensen, L. H. (1987) in *Iron–Sulfur Protein Research* (Matsubara, H., Katsube, Y., & Wada, K., Eds.) pp 3–21, Springer-Verlag, New York.

Jesson, J. P. (1973) in *NMR of Paramagnetic Molecules* (La Mar, G. N., Horrocks, W. D., Jr., & Holm, R. H., Eds.) pp 1–51, Academic, New York.

Kassner, R. J., & Yang, W. (1977) *J. Am. Chem. Soc. 99*, 4351–4355.

Krishnamoorthi, R., Markley, J. L., Cusanovich, M. A., Przysiecki, C. T., & Meyer, T. E. (1986) *Biochemistry 25*, 60–67.

Lecomte, J. T. J., & La Mar, G. N. (1986) *Eur. Biophys. J. 13*, 373–381.

Markley, J. L., Chan, T.-M., Krishnamoorthi, R., & Ulrich, E. L. (1987) in *Iron–Sulfur Protein Research* (Matsubara, H., Katsube, Y., & Wada, K., Eds.) pp 167–184, Springer-Verlag, New York.

Nagayama, K., Ohmori, D., Imai, T., & Oshima, T. (1987) in *Iron–Sulfur Protein Research* (Matsubara, H., Katsube, Y., & Wada, K., Eds.) pp 125–138, Springer-Verlag, New York.

Orme-Johnson, W. H., & Orme-Johnson, N. R. (1982) in *Iron–Sulfur Proteins* (Spiro, T. G., Ed.) Chapter 2, Wiley-Interscience, New York.

Palmer, G., Dunham, W. R., Fee, J. A., Sands, R. H., Izuka, T., & Yonetani, T. (1971) *Biochim. Biophys. Acta 115*, 711–715.

Phillips, W. D., & Poe, M. (1973) in *Iron–Sulfur Proteins* (Lovenberg, W., Ed.) Vol. II, pp 255–285, Academic, New York.

Poe, M., Phillips, W. D., Glickson, J. D., McDonald, C. C., & San Pietro, A. (1971) *Proc. Natl. Acad. Sci. U.S.A. 68*, 68–71.

Redfield, A. G., Kunz, S. D., & Ralph, E. K. (1975) *J. Magn. Reson. 19*, 116–118.

Salmeen, I., & Palmer, G. (1972) *Arch. Biochem. Biophys. 150*, 767–773.

Sanders-Loehr, J. (1988) in *Metal Clusters in Proteins* (Que, L., Jr., Ed.) pp 49–67, American Chemical Society, Washington, DC.
Sheridan, R. P., Allen, L. C., & Carter, C. W., Jr. (1981) *J. Biol. Chem. 256*, 5052–5057.
Thanabal, V., de Ropp, J. S., & La Mar, G. N. (1986) *J. Am. Chem. Soc. 108*, 4244–4245.
Thanabal, V., La Mar, G. N., & de Ropp, J. S. (1988) *Biochemistry 27*, 5400–5407.
Thomson, A. J. (1985) in *Metalloproteins, Part 1* (Harrison, P. M., Ed.) Chapter 3, Macmillan, London.
Tsukihara, T., Fukuyama, K., Nakamura, M., Katsube, Y., Tanaka, N., Kakudo, M., Wada, K., Hase, T., & Matsubara, H. (1981) *J. Biochem. (Tokyo) 90*, 1763–1773.
Tsukihara, T., Fukuyama, K., & Katsube, Y. (1987) in *Iron–Sulfur Protein Research* (Matsubara, H., Katsube, Y., & Wada, K., Eds.) pp 59–68, Springer-Verlag, New York.
Unger, S. W., Lecomte, J. T. J., & La Mar, G. N. (1985a) *J. Magn. Reson. 64*, 521–526.
Unger, S. W., Jue, T., & La Mar, G. N. (1985b) *J. Magn. Reson. 61*, 448–456.
Werth, M. T., Kurtz, D. M., Moura, I., & Le Gall, J. (1987) *J. Am. Chem. Soc. 109*, 273–275.
Wüthrich, K. (1986) *NMR of Proteins and Nucleic Acids*, Wiley, New York.

Structure of Vancomycin and a Vancomycin/D-Ala-D-Ala Complex in Solution

Henriette Molinari[‡] and Annalisa Pastore*
EMBL, Meyerhofstrasse 1, 6900 Heidelberg, West Germany
Lu-yun Lian,[§] Geoffrey E. Hawkes,[∥] and Keith Sales[∥]
NMR Biological Center, University of Leicester, Leicester, England, and Queen Mary College, Mile End Road, London E1 4NS, England
Received December 5, 1988; Revised Manuscript Received September 11, 1989

ABSTRACT: Restrained molecular dynamics simulations were used to study the interactions between the glycopeptide antibiotic vancomycin and the dipeptide Ac-D-Ala-D-Ala. Restraints were obtained from a combination of homonuclear and heteronuclear two-dimensional NMR experiments (NOESY, ROESY, $^{1}H-^{15}N$ inverse correlation). The comparison between the structures obtained for vancomycin alone and for the complex suggests a new hypothesis on the binding mode of this system. The numerical simulations were not straightforward because vancomycin is made of building blocks for which standard force-fields are not available. The representation of unusual chemical environments is also mandatory. We believe that our extension of the force-field parameters to our system could be of more general interest. Furthermore, we consider vancomycin and its complex a good example for exploring the more general problem of molecular recognition, a challenge that has been widely approached in the past few years but for which no unique and general methodology has, so far, been recognized.

The glycopeptide antibiotic vancomycin (see structure I) from *Streptomyces orientalis*, first reported in 1956 (McCormick et al., 1956), is of interest not only for its renewed clinical importance as a therapeutic agent in the treatment of methicillin-resistant staphylococcal infections (Karchmer et al., 1983) but also because it represents one of the smallest peptide–peptide binding systems where specific and tight interaction is achieved. The bacteriocidal actions of many antibiotics are associated with the inhibition of cell-wall biosynthesis that results from the binding of the antibiotics to enzymes and intermediates in the cell-wall biosynthetic pathway (Strominger, 1969). It has been suggested (Rogers, 1969; Rogers & Forsberg, 1971) that when cell-wall biosynthesis is inhibited, the natural ongoing autolysis of the cell wall is no longer in balance with the insertion of new cell-wall material. The bacteriocidal effect of vancomycin, in the cell, is associated with the strong binding of vancomycin to the cell wall. This is likely to result in changes in the three-dimensional arrangements of the cell-wall polymers and in the contacts between the cell wall and protoplast membrane, thus affecting the relative rates of cell-wall autolysis and the insertion of new cell-wall material (Best & Durham, 1965). It is therefore of interest to study models of the binding mode of this antibiotic.

The complex between vancomycin and the dipeptide Ac-D-Ala-D-Ala is a simple good model to simulate the binding (Nieto & Perkins, 1971), since this dipeptide represents a common C-terminal unit in the cell walls of several bacterial species (Perkins, 1982). On the basis of the NMR data as well as of molecular modeling and chemical modifications, Williams and Convert, who first investigated the complex, have proposed the hydrogen-bonding pattern in the complex (Williams, 1984; Kannan et al., 1988; Convert et al., 1980). They assumed the rotation of the *N*-Met-leucine side chain as a driving force for the complexation, which would allow a closer intermolecular distance between the dipeptide carboxylate and the vancomycin ammonium group (see structure I).

Popieniek and Pratt (1988) have recently explored in more detail the kinetics and the mechanism of the binding of three

* To whom correspondence should be addressed.
‡ Permanent address: Dipartimento di Chimica Organica e Industriale, Via Golgi 19, 20133 Milano, Italy.
§ University of Leicester.
∥ Queen Mary College.

0006-2960/90/0429-2271$02.50/0